2015 IEEE International Conference on Robotics and Automation (ICRA)
Washington State Convention Center
Seattle, Washington, May 26-30, 2015

Dynamic Brace for Correction of Abnormal Postures of the Human Spine

Joon-Hyuk Park, Paul Stegall, Sunil K. Agrawal*

Abstract— **This paper describes the design and control architectures for a novel active thoracolumbosacral orthosis targeted at correction of abnormal postures and treatment of the human spine, often seen in adolescent idiopathic or neuromuscular scoliosis. Our novel device is motivated by the current limitations of the rigid braces used for this purpose which do not adapt to changes in the skeletal system in response to treatment. In addition, the dynamic brace can open possibilities for new treatment methods which currently do not exist. Previous brace designs were not capable of providing dynamic controlled forces.**

Our design utilizes two Stewart-Gough platforms in series, each controlled independently, either in position or force modes. The design can provide controlled forces/torques on different regions of spine to modify the posture. Additionally, it can control the motion of different regions of the spine through independent position control of each platform using six parallel actuators. Both control methods were validated in bench-top tests. A range of motion study was also performed with a healthy subject wearing the device while the system was controlled in transparent mode.

I. Introduction

Braces have been used to treat scoliosis since the 1500's with the use of padded iron corsets [1]. While it is a widely accepted practice in the treatment of idiopathic scoliosis, systematic, randomized, group studies on the effectiveness of spine braces have been performed only recently [2]. The results clearly show that spine braces help to curtail progression of the abnormal spine curves in adolescents and prevent surgery.

The current standard practice is that braces are composed of a single rigid body. Boston and Cheneau braces apply three-point forces with rotation [3], [4]. The Milwaukee brace is designed to provide traction and rotation to the spine [5]. The Charleston Brace is a night-time brace utilizing bending [6]. The goals of these braces are to correct or stop the progression of abnormal curvature of the spine.

The rigidity of these braces makes these difficult to wear for extended periods of time as they interfere with typical activities of daily living. To allow for greater mobility, a SpineCor brace was recently proposed which uses a series of elastic straps to correct the curvature with varying levels of success [7], [8]. However, this brace is relatively new and has not been widely adopted by orthotists. Even with increased mobility, the force application is still passive and requires extensive training to provide appropriate correction [9].

Authors are with Robotics and Rehabilitation (ROAR) Laboratory, Department of Mechanical Engineering in Columbia University, New York, NY 10027 (jp3350, prs2136, sunil.agrawal)@columbia.edu
*Corresponding Author

There have been limited efforts in active bracing. It has been shown by Mac-Thiong et al. that reduced strap tension lowers the brace's pressure against the body and reduces brace effectiveness [10]. This is important as strap tension varies throughout the day as the user moves and settles in the device [11]. Lou et al. created a pneumatic device capable of increasing or decreasing the pressure from a pad internal to the brace in order to achieve proper brace tension [12]. However, this method is limited in how the force between the brace and the human body can be modulated, as the net force does not generally scale with normal pressure. There has also been an effort towards motorized traction for lower back pain [13].

The novel brace presented in this paper is capable of applying both forces and moments to the body at two locations. The brace can control either the force and moments applied to the body or its position and orientation. If used in position control mode, the load cells can be used to evaluate the six dimensional forces/torques while achieving a certain level of correction. If used in force mode, the device can exert six dimensional corrective forces/torques on the body or zero force to the user in transparent mode.

II. Design

The design goal of the dynamic brace is to provide controlled motion or force at selected segments of the human spine. To accomplish this goal, the brace is made in three segments, using semi-rigid 0.25 cm fused deposition modeling (FDM) ABS, separated by a 4 cm gap in the neutral position. A subject's torso was scanned to create a 3D model which was then used to manufacture the three segments of the brace, Figure 1a. Each segment has a series of holes along the circumference at 10° increments. This allows flexibility in the placement of the actuator mounts which attach to some of the holes. The actuator mounts were also made from FDM ABS. The linear actuators are capable of a peak force of 55 N and a peak speed of 5 mm/s with a 5 cm stroke length (Firgelli, L12-50-210-12-P). At the base of each actuator, a load cell (Futek, LCM200) and a conditioning board (Mantracourt, ICA6H) are mounted. Each actuator has a universal joint at the base and a spherical joint at the top. The brace is lined with plastazote polyethylene foam for comfort.

The actuator's position feedback and load cell voltage are multiplexed and sent to the control board (National Instruments, sbRio-9626). The motors are driven at 12 V using a 1000Hz PWM signal through a small driver (Toshiba, TB6612FNG).

978-1-4799-6923-4/15/$31.00 ©2015 IEEE

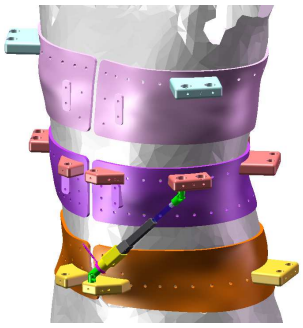

(a) Brace model on scanned figure.

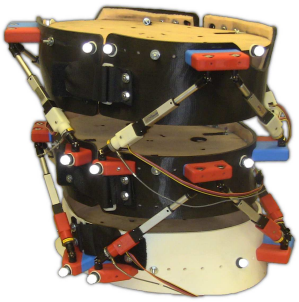

(b) Brace with internal supports.

Fig. 1: Brace development.

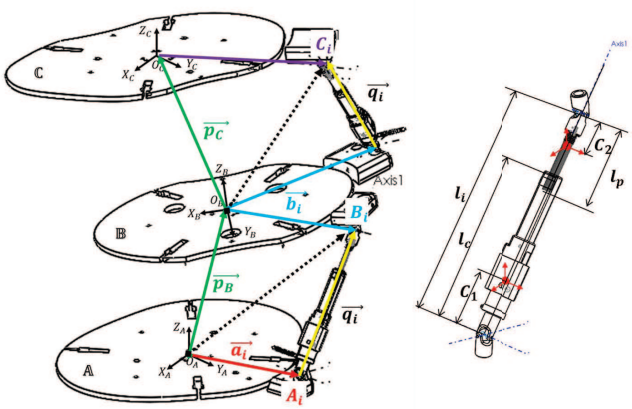

Fig. 2: Geometry and parameterization of Stewart platform

III. Modeling

A. Kinematics and Jacobian

The system consists of two parallel platforms connected in series. It has a total of twelve active degrees-of-freedom controlled by twelve linear actuators. The architecture of each parallel platform follows the kinematic structure of a 6-6 Stewart-Gough platform where all the limbs share identical kinematic chains of UPS, Figure 2. The parameterization and dynamics will be presented for only the lower parallel platform, which can also be extended to the top platform. Each limb connecting the fixed base $\mathbb{A}$ to the moving platform $\mathbb{B}$ forms a kinematic loop which can be expressed in the vector form as

$$\mathbf{q}_i = \mathbf{p_B} - \mathbf{a}_i + \mathbf{R_B}\mathbf{b}_i, \quad i = 1, .., 6 \tag{1}$$

with $\mathbf{p_B} = [P_Bx, P_By, P_Bz]^T$ a position vector and $\mathbf{R_B}$ a rotation matrix formed by three rotation angles$(\psi_B, \theta_B, \phi_B)$. $\mathbf{q}_i$ is a vector with magnitude q_i along a unit vector along the leg. $\mathbf{q} = [q_1, q_2, \ldots, q_6]^T$ is the vector of actuated joint coordinates and $\mathbf{X_B} = [P_Bx, P_By, P_Bz, \psi_B, \theta_B, \phi_B]^T$ is the vector of moving platform motion variables. The rotation of the moving platform is defined by pitch-roll-yaw angles about the axes of base platform coordinate frame[1].

For inverse kinematic analysis, the moving platform position $\mathbf{p_B}$ and orientation $\mathbf{R_B}$ are given and the problem is to solve for the joint variables, $\mathbf{L} = [l_1, l_2, l_3, l_4, l_5, l_6]^T$. The length of each limb l_i can be expressed as a norm of vector $\mathbf{q}_i$

$$l_i^2 = \mathbf{q}_i^T\mathbf{q}_i = [\mathbf{p_B} - \mathbf{a}_i + \mathbf{R_B}\mathbf{b}_i]^T[\mathbf{p_B} - \mathbf{a}_i + \mathbf{R_B}\mathbf{b}_i] \tag{2}$$

Hence, each limb length can be uniquely determined for given position and orientation of the moving platform.

For forward kinematic analysis, the joint variables l_i are given and the problem is to solve for $\mathbf{X}_B$ of the moving platform. In this study, an iterative numerical solver is used with screw axis representation of the rotation matrix [14], [15]. X_B is redefined with screw coordinates as

$$\mathbf{X_B} = [P_Bx, P_By, P_Bz, s_x, s_y, s_z, \Theta]^T \tag{3}$$

in which s_x, s_y, s_z, and Θ are obtained from rotation matrix

$$\begin{aligned} \Theta &= cos^{-1}\frac{r_{11} + r_{22} + r_{33} - 1}{2} \\ s_x = \frac{r_{32} - r_{23}}{2sin\Theta}, s_y &= \frac{r_{13} - r_{31}}{2sin\Theta}, s_z = \frac{r_{21} - r_{12}}{2sin\Theta} \end{aligned} \tag{4}$$

The seven equations to solve for forward kinematics are

$$\begin{aligned} E_i &= -l_i^2 + \mathbf{q_i}^T\mathbf{q_i} = 0 \\ &= -l_i^2 + [\mathbf{p_B} + \mathbf{R_B}\mathbf{b}_i - \mathbf{a}_i]^T[\mathbf{p_B} + \mathbf{R_B}\mathbf{b}_i - \mathbf{a}_i] = 0 \\ &\quad for\ i = 1, .., 6 \\ E_7 &= \hat{s} \cdot \hat{s} = s_x^2 + s_y^2 + s_z^2 = 1 \end{aligned} \tag{5}$$

The nonlinear least-square optimization routines were used to minimize $\frac{1}{2}\sum E_i$. The multiplicity of the solution is resolved by iteratively comparing the solution to the one obtained from a previous step. If the error is within a prescribed threshold, that solution is chosen.

The Jacobian matrices are computed from velocity loop closures which are directly obtained by differentiating Eqn (1) as follows

$$\dot{\mathbf{p_B}} = \dot{\mathbf{q}}_\mathbf{i} - \omega_\mathbf{B} \times \mathbf{R_B}\mathbf{b_i} \quad for\ i = 1, , 6 \tag{6}$$

in which angular velocity $\omega_\mathbf{B}$ of $\mathbb{B}$ with respect to $\mathbb{A}$ is

[1]First rotation about fixed x axis by ψ, followed by rotation about fixed y axis by θ, followed by rotation about fixed z axis by ϕ.

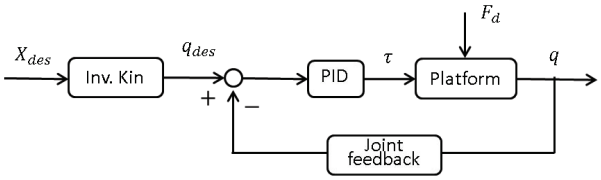

Fig. 3: A PID controller implemented in joint space for motion control. Inv. Kin stands for inverse kinematics.

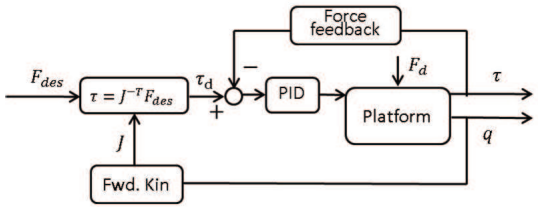

Fig. 4: A PID controller implemented in joint space for force control. Fwd. Kin stands for forward kinematics.

$$\omega_{\mathbf{B}} = \begin{bmatrix}\omega_1\\ \omega_2\\ \omega_3\end{bmatrix} = \begin{bmatrix}1 & 0 & -s\theta\\ 0 & c\psi & s\psi c\theta\\ 0 & -s\psi & c\psi c\theta\end{bmatrix}\begin{bmatrix}\dot{\psi}\\ \dot{\theta}\\ \dot{\phi}\end{bmatrix} \tag{7}$$

Jacobian has the following structure

$$\dot{L} = J\dot{X}_B, J = \begin{bmatrix}\hat{q}_1^T & (b_1 \times \hat{q}_1)^T\\ \hat{q}_2^T & (b_2 \times \hat{q}_2)^T\\ \hat{q}_3^T & (b_3 \times \hat{q}_3)^T\\ \hat{q}_4^T & (b_4 \times \hat{q}_4)^T\\ \hat{q}_5^T & (b_5 \times \hat{q}_5)^T\\ \hat{q}_6^T & (b_6 \times \hat{q}_6)^T\end{bmatrix}_{(6\times 6)} \tag{8}$$

The static wrench of the moving platform can be also obtained using Jacobian and applying principle of virtual work, assuming the limb applies a force only along the limb axis.

$$F = J^T\tau \tag{9}$$

in which $\tau = [\tau_1, \tau_2, \ldots, \tau_6]^T$ is the actuator force vector, and $F = [f_x, f_y, f_z, m_x, m_y, m_z]^T$ is the output wrench from the manipulator.

B. Dynamics

The dynamics of the system is determined using Lagrange's method applied to the limbs and the platform. For the limb dynamic model, each limb is considered to be a cylinder and a piston with the center of mass located at a distance of c_{i_1} and c_{i_2} from the bottom and the masses are denoted by m_{i_1} and m_{i_2}, respectively (Fig. 2). The kinetic and potential energy for the limbs and the platform are first derived followed by computation of Lagrangian. Once the equations of motion for the limb segments and the platform segment are obtained, the closed form dynamic equations of motion of the whole system are determined.[2].

IV. Controller

Two control modes were implemented to articulate the system: (i) motion control mode, (ii) force control mode. Each limb has built-in sensors to record its joint displacement or force applied by the joint actuator. This information is used by the closed-loop controller in both modes. The upper and lower parallel platforms have their own motion and force controllers which can be operated independently.

[2]Explicit expressions for dynamic equations are not provided in this paper for brevity, similar formulation can be found in [16], [17]

A. Motion Control

The control architecture for motion control is shown in Fig. 3. Since direct measurement of motion of the platform requires additional Cartesian motion sensors, the controller was developed in joint space using active joint position feedback. The desired motion of the platform X_d is mapped into the joint space variables q_d using inverse kinematics. The error is measured as the difference between the desired joint motion and the actual joint motion. These errors are a result of external disturbances or geometric mismatch in the model. A PID controller generates the joint torques necessary to drive each actuator and the controller gains were experimentally tuned.

B. Force Control

The control architecture for force control is shown in Fig. 4. It was also implemented in joint space and the Jacobian is used to compute the desired joint torques based on desired output force/moment of the platform which was computed in real time from limb position feedback and forward kinematics. This quasi-static control approach works well for our application where the bandwidth of both motion and force control is fairly low.

V. Evaluation

The position and force controllers were tested to determine their accuracy. In addition, a range of motion study was performed by a human subject with the force controller. The coordinate frame of the brace is oriented at the center of the bottom segment with the x-axis to the right, the y-axis towards the anterior, and the z-axis vertically upwards. The displacements and rotations reported are relative to the corresponding axes of the respective segments in the neutral position, in the bottom coordinate frame. Rotation angle ϕ, θ, and ψ are about z, y, and x respectively, following the same rotation sequence as in Sec. III. For tests without a person wearing the device, 0.25 cm plywood sheets cut to the brace's shape were placed inside the brace to improve rigidity.

A. Force Controller Validation

The force controller validation utilized a test bed where the middle and bottom segments were attached to each other using a 6 axis force/torque sensor (ATI, Mini45) in the brace's neutral position (Fig. 5). The brace was then driven to follow a force/torque profile: 1) one directional force

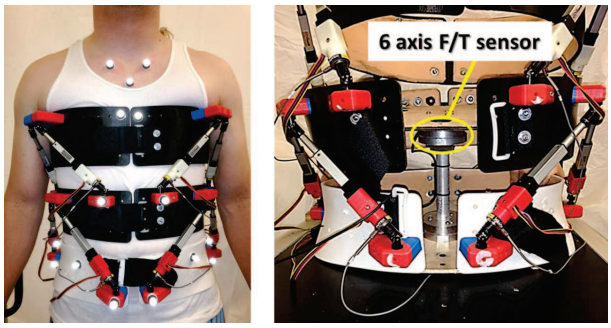

Fig. 5: (left) subject wearing the brace, (right) force evaluation test-bed with coordinate frame of the load cell. The central column connected the middle and bottom segments.

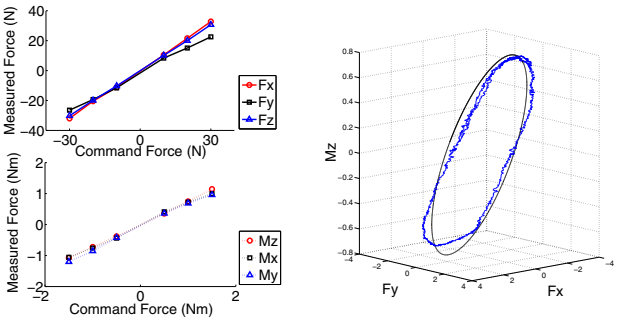

(a) Command and measured force in static pose

(b) Desired and measured force in Fx, Fy, Mz plane

Fig. 6: Graphical representation of the command force (dashed-black) and measured force (solid-blue) from ATI F/T sensor.

or torque; -30 N $\leq$ Fx, Fy, Fz $\leq$ 30 N and -1.5 Nm $\leq$ Mx, My, Mz $\leq$ 1.5 Nm, 2) three dimensional force/torque. The calculated force/torque from the load cells were then compared to the force/torque sensor to determine the sensor error, and the commanded force/torque profile to evaluate tracking error.

B. Position Controller Validation

The position controller was tested by moving the brace through a range of translation and rotation. Rotation about z and translation about y in the transverse plane was tested, denoted as three-point mode, as this mimics traditional three-point correction in spine braces. Flexion and lateral bending were tested to compare bending in a brace. The last series of tests were for isolated translations and rotations. For both, the upper Stewart Platform either performed the same task (follow) or the opposite task (mirror) as the lower Stewart Platform. The motion was recorded through potentiometers on the motors as well as a motion capture system (Vicon, Bonita). The translation and rotation of the middle and top segments relative to the neutral position were recorded and analyzed in the bottom coordinate frame.

C. Range of Motion Testing

The range-of-motion (ROM) was tested to determine the motion allowed by the brace in transparent mode (zero desired force). A healthy individual, without scoliosis, had markers placed on their anterior superior iliac spines, sacrum, sternoclavicular joints, and the inferior border of the manubrium. The subject bent to his maximum in the frontal (lateral bending), sagittal (flexion/extension), and transverse (vertical rotation) planes. The maximum change in the angle between the pelvis and the sternum were then compared for all three motions with and without the brace.

VI. Results and Discussion

A. Force Controller Results

The force controller was able to follow the commanded force/torque (f/t) profile for one directional inputs with less than 4% average error, see Figure 6a. Three dimensional f/t profile showed slightly larger errors compared to the one directional f/t test but still within an acceptable error

TABLE I: Orientation error of middle and top segments of seven modes

Middle	ϕ (deg)	θ (deg)	ψ (deg)
three-point	0.37 ± 0.43	0.18 ± 0.12	0.23 ± 0.21
flexion	0.07 ± 0.05	0.15 ± 0.10	0.43 ± 0.27
lateral bending	0.14 ± 0.08	0.29 ± 0.27	0.21 ± 0.16
rotation follow	0.09 ± 0.08	0.15 ± 0.13	0.18 ± 0.13
rotation mirror	0.07 ± 0.05	0.17 ± 0.14	0.18 ± 0.14
translation follow	0.08 ± 0.04	0.04 ± 0.03	0.12 ± 0.08
translation mirror	0.10 ± 0.02	0.05 ± 0.02	0.10 ± 0.06
Top			
three-point	0.07 ± 0.04	0.18 ± 0.11	0.22 ± 0.13
flexion	0.16 ± 0.09	0.09 ± 0.06	0.98 ± 0.63
lateral bending	0.40 ± 0.21	0.55 ± 0.51	0.46 ± 0.22
rotation follow	0.15 ± 0.15	0.23 ± 0.20	0.17 ± 0.24
rotation mirror	0.11 ± 0.09	0.12 ± 0.10	0.15 ± 0.09
translation follow	0.06 ± 0.04	0.05 ± 0.05	0.18 ± 0.13
translation mirror	0.14 ± 0.03	0.06 ± 0.06	0.14 ± 0.08

TABLE II: Position error of middle and top segments of seven modes

Middle	x (mm)	y (mm)	z (mm)
three-point	0.52 ± 0.34	1.13 ± 1.22	0.65 ± 0.36
flexion	0.59 ± 0.31	1.28 ± 0.71	0.57 ± 0.38
lateral bending	1.35 ± 0.73	0.28 ± 0.16	0.85 ± 0.54
rotation follow	0.67 ± 0.67	0.83 ± 0.47	0.55 ± 0.27
rotation mirror	0.73 ± 0.67	0.88 ± 0.52	0.72 ± 0.35
translation follow	0.26 ± 0.12	0.42 ± 0.20	0.32 ± 0.18
translation mirror	0.23 ± 0.12	0.47 ± 0.26	0.32 ± 0.25
Top			
three-point	0.53 ± 0.39	0.61 ± 0.48	1.18 ± 0.57
flexion	0.54 ± 0.44	6.99 ± 3.77	1.55 ± 0.89
lateral bending	6.74 ± 3.90	0.84 ± 0.52	1.46 ± 1.23
rotation follow	2.02 ± 1.22	2.54 ± 1.29	0.80 ± 0.39
rotation mirror	1.29 ± 0.72	1.51 ± 0.82	1.06 ± 0.47
translation follow	0.85 ± 0.60	0.93 ± 0.49	0.46 ± 0.26
translation mirror	0.31 ± 0.26	0.25 ± 0.24	0.73 ± 0.39

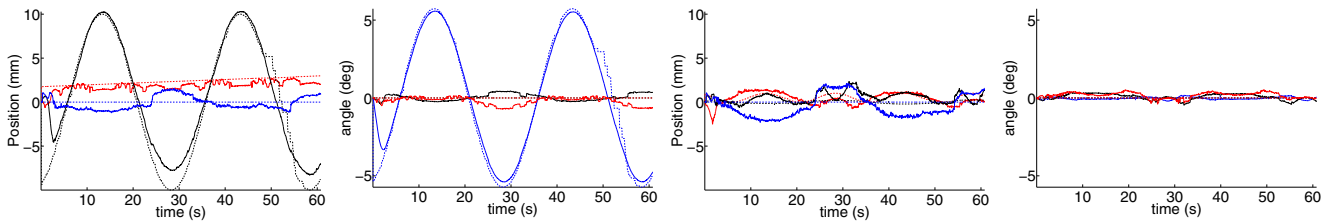

(a) XYZ position of the middle segment origin (b) Rotation angles of the middle segment. (c) Position of the top segment origin (d) Rotation angles of the top segment.

Fig. 7: Graphical representation of the command (dashed) and Vicon (solid) results from the three-point mode test. Rotation and translations about x, y, and z are represented by red, black, and blue respectively.

range ($\leq 7\%$), see Figure 6b. The compliance in the device seems to be the main source of error in three dimensional f/t testing as slight deformation from the brace was observed. Any structural deformation would likely result in changes in geometry which is difficult to capture and be reflected for real time control, hence, it will be desirable to identify where such deformation is likely to occur and increase the local stiffness in that area.

B. Position Controller Results

The position controller was able to follow all paths with less than 0.98° of average error for all tested trajectories, see Table I. For translational motions, the average positioning errors were sub-millimeter. With rotational paths, average positioning error was higher for both platforms, while still within the millimeter range, see Table II. These errors were most marked in the top segment, as errors from the middle segment would also appear here. Compliance in the device again seems to be a likely source of error, however, this should appear for both rotational and translational trajectories. An alternative explanation would be mismatch between the initial configuration of the model and the actual system. For flexion, if the distance between the middle and the top segment was larger than modeled, then for a rotation of the middle segment, the top segment would translate more in the y and z directions than expected; similarly if the distance was smaller the translation would be lower than expected resulting in greater error. This appears for both flexion (y, z) and lateral bending(x, z). Improved calibration could potentially reduce these errors. The top segment was capable of remaining nearly stationary while the middle brace was moved, see Figure 7c and Figure 7d. The brace was also capable of being robust to disturbances as seen in the initial offsets and recovery in Figures 7a and 7b.

C. Range of Motion Testing

In most cases, the device was capable of providing more than 75% of the subject's normal range of motion (ROM), this was not the case for rotation to the right, Table III. This reduction could result from the rigidity of the brace in the area it covers, restricting a small subset of the vertebrae while allowing motion in the uncovered regions. Extension was also notably reduced. A possible cause may be the tendency to inhale when extending and thereby increasing the tension in the brace. Further testing may need to be done to rule this out as a cause. The subject under testing has low flexion and rotation ranges compared to Doriot and Wang's data for young males [18]. This could possibly lead to a different result for individuals with a greater normal ROM, however, the ROM presented here is still increased over rigid braces.

TABLE III: Range of Motion in transparent mode

	No Brace (deg)	With Brace (deg)	Percent ROM
Flexion	36.9	37.0	100
Extension	24.9	19.1	76.4
Bending Right	43.0	35.6	82.6
Bending Left	41.5	38.7	93.1
Rotation Right	38.0	22.2	58.3
Rotation Left	42.8	34.5	80.8

VII. Limitations

The current design is not as low profile as currently used braces made out of sheets of thermomolded plastic. This was unavoidable in the first iteration where off-the-shelf commercial motors were used. Compliance with bracing regimens continues to be a hurdle as many individuals do not comply with the prescribed 12-16 hours of wear per day due to social stigma. While a bulkier brace would seem to be more visible and therefore less likely to be adopted, it is hoped that through appropriate control strategies the time the brace needs to be worn can be reduced without negatively impacting outcomes. If a wearer can receive the same quality of care while only wearing the brace at home, instead of wearing conventional braces for a majority of the day, then compliance may increase and individuals may be more likely to benefit from bracing, as it has been shown by Hassler, Wietlisbach, and Büchler that flexible bracing does not improve compliance if still requiring long duration wear [19].

VIII. Future Work

The dynamic brace is the first brace of its kind and will hopefully pave the way for future dynamic braces in this area. There are a number of improvements that can be made

to this brace in the future. Currently, the FDM ABS is brittle for day-to-day wear and FDM in not an economically viable manufacturing process compared to sheet forming. One of the next steps will be to move to sheet formed polyethylene in-line with current fabrication techniques. With this the control board and other electronics should be made compact so that the system becomes wearable.

Further testing needs to be done to evaluate the effectiveness of the proposed control strategies compared to traditional bracing techniques. The brace should also be utilized to do pilot studies for spinal correction as a part of future evaluations. The brace can be used in position mode under x-ray to determine the stiffness of the spine, rib cage, and soft tissues together under 6 DOF loading to better inform how forces should be applied through dynamic or rigid braces.

Additional sensors are planned to be implemented within the device. Force sensing resistors will be placed around the inner surface of the brace to measure the interaction forces between the device and the body during operation. Together with the load sensors placed at each actuator, force mapping between the actuator force and the force exerted on human body may be achievable qualitatively. It can also help prevent excessive local pressure applied to the body from the device by real time monitoring. Position and orientation sensors will be added to the brace to reduce the computational load in computing the forward kinematics and can potentially be used to capture user intention for active motion adaptation of the device.

IX. Conclusion

This paper presents a novel dynamic spinal brace, particularly targeting Scoliosis treatment. The motivation of this study comes from the limitations in current bracing therapy usually practiced with rigid braces for correction of the spine. Our goal was to design a brace that is dynamic in nature which has controllable motions and forces. This was done through implementing two layers of Stewart-Gough platforms in series and independently controlling each layer's motions or forces. Experimental evaluation of motion and force control was performed which showed a good performance on the developed controllers. Furthermore, human wearability testing was conducted while the device was in transparent mode. It was shown that more than 75% of natural range of motion was still retained while wearing the device. This study mainly focused on the technical aspects of the device, hence, further studies will also involve clinical testing to address the efficacy of the device in Scoliosis treatment.

Acknowledgments

The authors would like to thank John Tunney of East Coast Orthotics for performing the 3D scans used to make the brace. Additionally, we appreciate discussions with Dr. David Roye, a professor of Pediatric Orthpedics at Columbia University.

References

[1] R. Fayssoux, R. Cho, and M. Herman, "A history of bracing for idiopathic scoliosis in north america," *Clinical Orthopaedics and Related Research*, vol. 468, no. 3, pp. 654–664, 2010.

[2] S. L. Weinstein, L. A. Dolan, J. G. Wright, and M. B. Dobbs, "Effects of bracing in adolescents with idiopathic scoliosis," *New England Journal of Medicine*, vol. 369, no. 16, pp. 1512–1521, 2013. PMID: 24047455.

[3] J. Wynne, "The boston brace system philosophy, biomechanics, design & fit.," *Studies in health technology and informatics*, vol. 135, pp. 370–384, 2007.

[4] M. Rigo and H. Weiss, "The chêneau concept of bracing-biomechanical aspects," *Studies in Health Technology and Informatics*, vol. 135, p. 303, 2008.

[5] W. P. Blount, "The milwaukee brace in the treatment of the young child with scoliosis," *Archives of Orthopaedic and Trauma Surgery*, vol. 56, no. 4, pp. 363–369, 1964.

[6] C. T. PRICE, D. S. SCOTT, F. E. REED JR, and M. RIDDICK, "Night-time bracing for adolescent idiopathic scoliosis with the charleston bending brace: preliminary report," *Spine*, vol. 15, no. 12, pp. 1294–1299, 1990.

[7] C. Coillard, V. Vachon, A. B. Circo, M. Beauséjour, and C. H. Rivard, "Effectiveness of the spinecor brace based on the new standardized criteria proposed by the scoliosis research society for adolescent idiopathic scoliosis," *Journal of Pediatric Orthopaedics*, vol. 27, no. 4, pp. 375–379, 2007.

[8] M. S. Wong, J. C. Cheng, T. P. Lam, B. K. Ng, S. W. Sin, S. L. Lee-Shum, D. H. Chow, and S. Y. Tam, "The effect of rigid versus flexible spinal orthosis on the clinical efficacy and acceptance of the patients with adolescent idiopathic scoliosis," *Spine*, vol. 33, no. 12, pp. 1360–1365, 2008.

[9] C. H. Rivard, "Letters," *Spine*, vol. 33, no. 25, p. 2837, 2008.

[10] J.-M. Mac-Thiong, Y. Petit, C.-É. Aubin, S. Delorme, J. Dansereau, and H. Labelle, "Biomechanical evaluation of the boston brace system for the treatment of adolescent idiopathic scoliosis: relationship between strap tension and brace interface forces," *Spine*, vol. 29, no. 1, pp. 26–32, 2004.

[11] C.-É. Aubin, H. Labelle, A. Ruszkowski, Y. Petit, D. Gignac, J. Joncas, and J. Dansereau, "Variability of strap tension in brace treatment for adolescent idiopathic scoliosis," *Spine*, vol. 24, no. 4, pp. 349–354, 1999.

[12] E. Lou, S. Venkateswaran, D. L. Hill, J. V. Raso, and A. Donauer, "An intelligent active brace system for the treatment of scoliosis," *Instrumentation and Measurement, IEEE Transactions on*, vol. 53, no. 4, pp. 1146–1151, 2004.

[13] E. D. LLC, "Exo dynamics products." `http://www.exodynamicsmedical.com/products/`, 2013. Accessed: 2014-09-29.

[14] J. Merlet, "Direct kinematics of parallel manipulators," *IEEE Transactions on Robotics and Automation*, vol. 9, no. 6, pp. 842–845, 1993.

[15] C. Innocenti, "A novel numerical approach to the closure of the 6-6 stewart platform mechanism," *In Proc. of the Fifth International Conference on Advanced Robotics*, pp. 852–855, 1991.

[16] H. Taghirad, "Parallel robots," *CRC press*, 2012.

[17] L.-W. Tasi, "Robot analysis," *John Wiley & Sons, Inc*, 1999.

[18] N. Doriot and X. Wang, "Effects of age and gender on maximum voluntary range of motion of the upper body joints," *Ergonomics*, vol. 49, no. 3, pp. 269–281, 2006.

[19] C. C. Hasler, S. Wietlisbach, and P. Büchler, "Objective compliance of adolescent girls with idiopathic scoliosis in a dynamic spinecor brace," *Journal of children's orthopaedics*, vol. 4, no. 3, pp. 211–218, 2010.